

On the Baldwin Effect in Active Galactic Nuclei:

I. The Continuum-Spectrum - Mass Relationship

A. Wandel¹

Racah Institute, The Hebrew University, Jerusalem 91904, Israel

ABSTRACT

We suggest that the Baldwin effect is a result of the spectral dependence of the line-driving ionizing continuum on the black hole mass. We derive a relationship between the mass of the central black hole and the broad emission-line luminosity in active galactic nuclei (AGN). Assuming the UV spectrum of AGN is emitted from an optically thick medium we find an expression for the characteristic energy of the "UV bump" in terms of the observable luminosity and emission-line width. We show empirically and analytically that the bump energy is anti-correlated with the black-hole mass and with the continuum luminosity. Our model reproduces the observed inverse correlation between equivalent width and continuum luminosity, yielding an explanation of the Baldwin effect from first principles. The model gives a good fit to the Baldwin effect of the CIV line for a mean quasar EUV spectrum (Zheng *et al.* 1997) and for several model spectra. The model also predicts a correlation between the strength of the Baldwin effect (the slope of the equivalent width as a function of luminosity) and the ionization potential, consistent with recent data.

Subject headings: galaxies: active — galaxies: nuclei — galaxies: Seyfert — quasars: general — black hole physics — accretion disks

1. INTRODUCTION

Baldwin (1977) showed that the equivalent width of the CIV emission-line decreases with increasing continuum luminosity, a correlation known as the 'Baldwin effect'. This result has been confirmed for a large set of AGN and a wide luminosity range (Kinney, Rivolo and Koratkar 1990). A similar relation has been found also for other broad emission-line s. Several models have been proposed to explain the Baldwin effect , such as a decrease of the ionization parameter or of the covering factor with luminosity (Wu, Boggess and Gull 1983) or the accretion disk inclination

¹On leave at Astronomy Department, University of California, Los Angeles, CA 90095-1562

(Netzer 1985). Nevertheless, the origin of the Baldwin effect is still not understood (for a recent review see Shields and Osmer, 1998).

The widest accepted explanation for the energy source of quasars and Active Galactic Nuclei (AGN) is the accretion of matter onto a supermassive black hole in the center of the host galaxy. The central mass implied by a variety of observations (see Wandel 1998) is of the order of $10^6 - 10^9 M_\odot$. The angular momentum directs the accreted material to form a disk around the central black hole and the properties of such an accretion disk may be calculated under a few basic assumptions (e.g. Sakura and Sunyaev, 1973). In particular one can calculate the luminosity and spectral distribution of the radiation from the accretion disk, given the black hole mass and the accretion rate.

The thermal emission from the accretion disk around a central mass of the size implied for AGN peaks in the UV, and ionizes the broad emission-line gas. The precise shape of the continuum spectrum from an accretion disk depends (among other factors) on the central mass. Since the continuum radiation ionizes the line-emitting material and drives the broad AGN emission-lines, the emission-line strengths depend on the continuum spectrum and therefore on the central mass.

In particular the spectral shape of the ionizing radiation can determine the equivalent width (the ratio between the energy flux in the line to the continuum energy flux at the line frequency) of the emission-line s.

We suggest that the Baldwin effect is a result of the spectral dependence of the line-driving ionizing continuum on the black hole mass. In the next section we present constraints on the black hole mass; section 3 describes the temperature and spectrum of the basic thin accretion disk model. Section 4 gives an empirical relation between the model parameters (M and \dot{M}) and the *observed* spectrum and luminosity, while section 5 relates these parameters to the *calculated* spectrum for various accretion disk models. In section 6 we derive the dependence of the line luminosity on the physical conditions in the gas. In section in 7 we compose all these elements to produce a relation between the equivalent width and the mass, and in section 8 we show that the model predictions are indeed consistent with the observed Baldwin effect for CIV and other lines.

2. Basic relations for accreting Black Holes

Any compact, accretion powered radiation source must obey several fundamental relations:

a. The Eddington limit: in order to maintain steady spherical accretion the luminosity must be less than the Eddington luminosity,

$$L < L_{Edd} = 4\pi GMm_p c / \sigma_T = 1.310^{46} M_8 \text{ erg/sec}$$

or

$$M_8 = 0.7\eta^{-1}L_{46} \quad (1)$$

where $M_8 = M/10^8 M_\odot$, $\eta = L/L_{Edd}$ is the Eddington ratio, and $L_{46} = L/10^{46}$ erg/sec.

b. The black body temperature: if a luminosity L comes from a region of radius R and temperature T , then

$$L < 4\pi R^2 \sigma T^4. \quad (2)$$

If a spectral feature at a photon energy of E is due to black body emission from a region of size R , then the temperature is given by $E \approx 3kT$, and $E \approx (10 \text{ eV})(T/10^5 \text{ K})$, so that

$$E \sim < (10 \text{ eV})L_{46}^{1/4}M_8^{-1/2}(R/5R_s)^{-1/2}. \quad (3)$$

and reversing the relation above we have an lower limit on the black hole mass (for a true black body spectrum this becomes an approximate equality):

$$M_8 \sim > 2E_{Ryd}^{-2}L_{46}^{1/2}(R/5R_s)^{-1} \quad (4)$$

where $R_s = 2GM/c^2 \approx 3 \cdot 10^{13} M_8$ cm is the Schwartzshild radius and E_{Ryd} is the spectral energy in Rydbergs. (Note that L_{46} is the bolometric luminosity; if the observed (say optical) luminosity is used, a bolometric correction must be included).

Combining eqs. 1 and 4 we can eliminate M obtaining (for black body emission) an estimate of the size:

$$\frac{R}{R_s} \approx 13L_{46}^{-1/2}\eta E_{Ryd}^{-2} \quad (5)$$

c. Variability: the shortest time scale for global variations in the luminosity is the light travel time across the Schwartzshild radius, hence if the luminosity is observed to vary significantly on a time scale δt , the black hole mass has to be

$$M_8 < \frac{\delta t}{10^3 r \text{sec}}, \quad (6)$$

where r is the effective radius of emission in units of R_s .

However, for continuum changes near the feature of spectral energy E the light travel time is (from eq. 5)

$$\delta t_l \approx \frac{R}{c} \approx 1.5L_{46}^{1/2}E_{Ryd}^{-2} \text{days}, \quad (7)$$

and the dynamical time is

$$\delta t_d \approx \frac{R}{v} \approx 20L_{46}^{1/4}\eta^{1/2}E_{Ryd}^{-3} \text{days}, \quad (8)$$

which gives time scales of the order of the observed UV variability in Seyferts and quasars.

3. The thin accretion-disk model

Many authors have tried to fit accretion disk spectra to the observed AGN continuum, implying the accretion disk parameters (M, \dot{M}, α) and the black hole spin (e.g. Schwartzschild or Kerr) which give the best fit to the observed optical-UV continuum (e.g. Wandel and Petrosian 1988; Sun and Malkan 1989; Laor 1990).

3.1. The accretion disk spectrum

The radiative energy output of the accretion disk is dominated by the release of gravitational potential energy, the rate of which is $GMM\dot{r}/r$. A more accurate calculation yields for the flux emitted per unit area

$$L(R) = \frac{3GMM\dot{r}}{8\pi R^3} \left[1 - \left(\frac{R_{in}}{R} \right)^{1/2} \right] \quad (9)$$

where R_{in} is the inner disk radius. In the outer part of the thin disk the opacity is dominated by true absorption and the local spectrum is a black body spectrum. For this part of the disk, comparing eq. 9 to the black body radiation flux gives for the disk surface temperature

$$T(R) \approx \left(\frac{3GMM\dot{r}}{8\pi\sigma R^3} \right)^{1/4} \approx 6 \cdot 10^5 \left(\frac{\dot{m}}{M_8} \right)^{1/4} r^{-3/4} \text{ K} \quad (10)$$

where $r = R/R_s$ and

$$\dot{m} = \dot{M}/\dot{M}_{Edd} \approx 2(M/M_\odot \text{yr}^{-1})M_8^{-1}(\epsilon/0.1)^{-1}$$

is the accretion rate in units of the Eddington accretion rate, $\dot{m} = 1$ at the Eddington limit. When the accretion rate approaches the Eddington rate, the intermediate disk region becomes dominated by electron-scattering, the spectral function will be of a modified black body and the surface temperature is higher than given by eq. 10. At still smaller radii, the pressure in the disk is dominated by radiation pressure, rather than by gas pressure, and the thin disk solution becomes thermally unstable. In that inner region the thin disk solution is probably not valid, and has to be replaced by a hot disk solution (e.g. Wandel and Liang 1991). It turns out that the intermediate modified black body region is relatively narrow, and close to the black body - electron scattering boundary the spectrum is nearly a black body one, so both regimes may be approximated by the black body solution.

The spectrum of a multi- black body accretion disk is given by integrating over the entire disk,

$$L_\nu \approx \int_{R_t}^{R_{out}} 2\pi R B_\nu[T(R)] dR \quad (11)$$

where $B_\nu(T)$ is the Planck function and R_t is the transition radius from the intermediate to the inner radiation-pressure dominated region (for $\dot{m} < 0.02$ the black body region extends down to the inner edge of the disk and $R_t = R_{in}$).

Since the $B_\nu(T)$ has a sharp peak at $h\nu_{co} \approx 3kT$ and cuts off at higher frequencies, the highest frequency of the black body part of the disk spectrum comes from the radius R_t , with the highest temperature for which the disk is still optically thick. Eq. 11 gives a spectrum which depends on the radial extent of the black body part of the disk. If that part is extended ($R_{out}/R_t \gg 1$) the spectrum is almost flat ($\sim \nu^{1/3}$) and cuts off beyond $h\nu_{co} \approx 3kT(R_t)$ (or $3kT(5R_S)/h$ for $\dot{m} < 0.1$). If $R_{out}/R_t \sim$ a few, the spectrum will be merely a somewhat broadened Planck spectrum, but if the accretion disk is extended over a large radial range there is a significant flat part. In that case a better approximation than the Planck spectrum is

$$L_\nu \approx A \left(\frac{\nu}{\nu_{co}} \right)^{1/3} \exp \left(-\frac{\nu}{\nu_{co}} \right) \quad (12)$$

where A and ν_{co} are the normalization and cutoff frequency. For a Kerr black hole Malkan (1990) finds $\nu_{co} = (2.9 \times 10^{15} \text{ Hz}) \dot{M}_{0.1}^{1/4} M_8^{-1/2}$, where $\dot{M}_{0.1} = \dot{M}/0.1 M_\odot \text{ yr}^{-1}$. This can be written as

$$h\nu_{co} = (6 \text{ eV}) \dot{M}^{1/4} M_8^{-1/4} = (20 \text{ eV}) L_{46}^{1/4} M_8^{-1/2} \quad (13)$$

(note that here L_{46} is the *observed* luminosity, and we have included a bolometric correction of 10. Also note that for a Kerr black hole the efficiency in the definition of \dot{m} is $\epsilon = 0.4$). The relation between the cutoff frequency and the inner disk temperature in the two cases of face-on Kerr and the black body approximation is

$$h\nu_{co} = 0.64kT_{max} = 2.5kT_{BB}$$

(Malkan 1990).

Although the soft X-ray excess suggest a higher thermal temperature in some objects, In general the characteristic temperature is likely to be related to the UV spectrum; While in the UV spectrum is produced by thermal emission from an optically thick gas (with eventual reprocessing), the X-rays are more likely to be produced by a hotter medium due to processes such as Comptonization, a two-temperature disk (Wandel and Liang 1991) or hot corona (Haardt, Maraschi and Ghisellini 1994; Czerny, Witt and Zycki 1996).

4. Deriving M and \dot{M} from the UV spectrum

We want to find an approximate relation between the black hole mass and accretion rate and the continuum spectrum. The accretion rate is determined straightforwardly by the luminosity, via the relation $L_{ion} = \epsilon f_{ion} \dot{M} c^2$, where f_{ion} is the fraction of the ionizing out of the total luminosity. To estimate the black hole mass we may use the multi-black body accretion disk spectrum. As

discussed in the previous subsection the UV bump cutoff frequency is determined by the highest surface temperature in the black body part of the disk. If the black body region extends down to a radius R_t , and the EUV cutoff energy is E_{co} , then eq. 4 gives (we assume the inner region is optically thin and much hotter, so its contribution in the frequencies of interest can be neglected)

$$M_8 \approx 2.5(E_{co}/10\text{eV})^{-2}L_{46}^{1/2}(R_t/5R_s)^{-1}. \quad (14)$$

In several accretion disk models the black body regime extends close to the inner disk edge. This is the case in the “ β ” disk model with viscosity proportional to the gas pressure ($\nu \sim \beta P_{gas}$). For low accretion rates ($\dot{m} < 0.1$) this is true also for the “ α ” model with viscosity proportional to the total pressure ($\nu \sim \alpha(P_{gas} + P_{rad})$). In this case, since the disk emissivity peaks at $R \approx 5R_S$ (for a non-rotating black hole) we may use eq. 3 in order to find the cutoff energy.

$$E \sim > (17 \text{ eV})L_{46}^{1/4}M_8^{-1/2} \quad \text{Schwartzshild} \quad (15)$$

(where we have introduced a bolometric correction $L_{opt} = 0.1L_{bol}$).

The equivalent result for a Kerr black hole (eq. 13) is very similar:

$$E \sim > (20 \text{ eV})L_{46}^{1/4}M_8^{-1/2} \quad \text{Kerr.}$$

Plotting the cutoff frequency versus the luminosity one can infer the mass, and vice versa, if the mass can be estimated independently, it is possible to estimate the cutoff frequency (fig. 1).

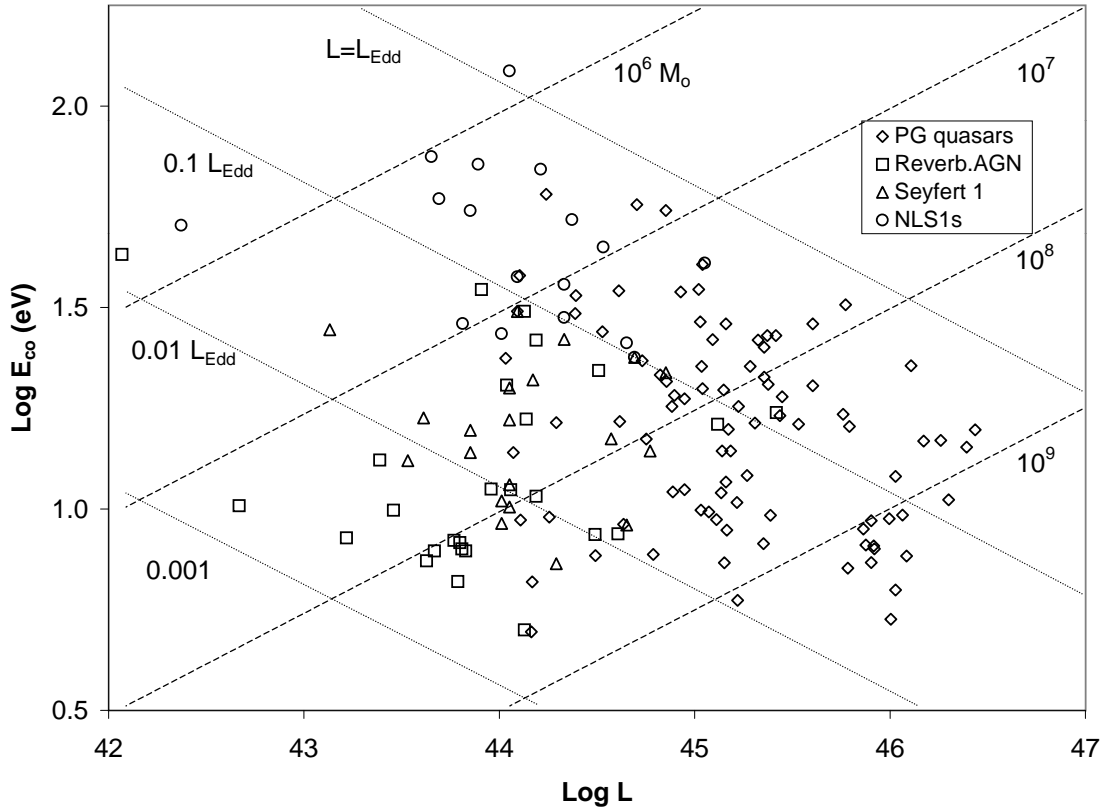


Figure 1. The cutoff energy (for an accretion disk spectrum vs. the monochromatic luminosity at 5100Å. Diagonal dashed lines indicate constant black hole masses, and diagonal dotted lines indicate the Eddington ratio. The data shown consists of PG quasars (diamonds; from Boroson and Green, 1994), Seyfert 1 galaxies (triangles and squares, the latter indicate AGN with BLR reverberation data from Wandel, Peterson and Malkan 1999, with luminosities modified for $H = 50$) and Narrow Line Seyfert 1s (Boller, Brandt and Fink, 1996)

It is possible to estimate the black hole mass from the broad emission line profile, assuming the velocity width is induced by a Keplerian velocity dispersion. When the broad line region size is estimated by reverberation mapping, this technique is particularly reliable. Wandel, Peterson and Malkan (1999) have used a sample of AGN with reverberation data to calibrate the mass

estimate obtained from photoionization models, finding the relation

$$M_8 \approx 0.4 \left(\frac{L_{46}}{Un_{10}} \right)^{1/2} v_3^2 \quad (16)$$

where U is the ionization parameter, n_{10} is the density in units of 10^{10} cm^{-3} and v_3 is the H β FWHM in 10^3 km s^{-1} . Using this calibrated relation makes it possible to estimate black hole mass estimates for large samples, even without reverberation data (Wandel, Malkan and Peterson, in preparation). Combining equations 16 and 13 or 15 we have

$$E_{co} \approx (40 \text{ eV}) (Un_{10})^{-1/4} v_3^{-1} \quad (17)$$

Note that the luminosity dependence cancels out, and the dependence on the unknown parameters U and n is weak. Using eq. 17 and the average fiducial value of $Un_{10}=1$ we find the mass and cutoff energy distribution for a large sample of quasars, Seyfert 1 galaxies and NLS1s (fig 1). Note that E_{co} is anticorrelated with the mass, and in particular that different AGN categories group in different regions in the $L - E_{co}$ plane: quasars have more massive black holes and low cutoff energies, Seyfert 1 galaxies have intermediate black hole masses ($10^7 - 10^8 M_\odot$), and NLS1s have low black hole masses ($10^6 - 10^7 M_\odot$) and high cutoff energies. This is consistent with the large soft X-ray excesses observed for many of the NLS1s (Boller, Brandt and Fink, 1996).

The diagonal dotted lines in fig. 1 give the L/L_{Edd} ratio - quasars are in the 0.01-1 range, Seyferts in the 0.001-0.1, and NLS1s are all near Eddington, $L/L_{Edd} \approx 0.1 - 1$.

A similar analyses for the Schwarzschild accretion disk has been performed by Wandel and Petrosian (1988), who calculated for each pair of accretion disk parameters M and \dot{M} the actual observables, e.g. the UV luminosity and spectral index.

5. Relating M and L to the Ionizing Spectrum

5.1. Temperature dependence of the Ionizing Spectrum

The ionizing power Q is essentially the photon flux above the ionization potential E_{ion} of the line in question - e.g. 1Ryd (13.6 eV) for Ly α and 48eV for CIV.

We shall now relate the ionizing flux (defined by $Q \propto L_{ion} / \langle E \rangle$) to the temperature of the continuum-emitting gas, assuming the emission is thermal (which is certainly true in the thin accretion disk model, and supported by the presence of the blue bump feature in the spectrum of most AGNs. If $E_{co} < E_{ion}$ this frequency is on the Wien part, and the flux is sensitively influenced by the effective disk temperature, T_{eff} . In the parameter range of interest we may therefore assume that the equivalent width is strongly correlated with T_{eff} . Quantitatively, the correlation

is related to the logarithmic derivative

$$\frac{d \ln B_\nu}{d \ln T} = \frac{-xe^x}{e^x - 1} \quad (18)$$

where $x = h\nu/kT$. For $kT < 1$ Ryd, which is true in a wide range of cases, as we show below, eq. 18 gives

$$\frac{d \ln B_\nu}{d \ln T} \approx -h\nu/kT,$$

namely a strong correlation with T.

In order to relate the UV ionizing spectrum near 1Ryd to the accretion parameters, it is necessary to determine the effective black body temperature of the emitting region, which we do in the next section.

Once this temperature is determined, we can estimate the ratio of fluxes in any two desired energy bands, in particular the flux in the ionizing energy band to the energy E_I of the emission-line in question, which is related the equivalent width, since the line luminosity is related to the ionizing flux. From eq. 12 we have

$$L_{\nu ion}/L_{\nu I} \approx (E_I/E_{ion})^{1/3} \exp[(E_I - E_{ion})/E_o]. \quad (19)$$

5.2. The Variability-Effective Temperature Relation

We have already derived a quite general temperature-radius relation for black body emission from an accretion flow (eq. 5). We can apply this relation to determine the temperature or radiation peak energy as a function of the observed luminosity and estimated mass.

In order to determine a characteristic temperature we need either indicate the size of the emitting region (and use eq. 2) or assume an emission model, as done below for the accretion disk model. The size of the emitting region can be bounded by variability analyses. From eqs. 2 and 6 we have

$$L < 4\pi\sigma c^2(\delta t)^2 T^4$$

which gives

$$E_{eff} > 10L_{46}^{1/4}(t_{day})^{-1/2} eV \quad (20)$$

where t_{day} is the variability scale in days. X-ray data imply a linear relation between luminosity and variability time in AGN (Barr and Mushotzky, 1986, Ulrich, Maraschi and Urry 1997). Recently a time scale of the order of 30 days has been found in the X-ray PDS of NGC 3516 (Edelson and Nandra 1999), but the fastest variability observed in AGN is of the order of hours. Assuming a relation, $t_{day} \sim \tau_L L_{46}$, eq. 20 gives

$$E_{eff} > (10 eV) \tau_L^{-1/2} L_{46}^{-1/4}. \quad (21)$$

For a linear $M - L$ relation $L_{46} \approx (\eta/0.1)M_8$ (e.g. Wandel and Yahil 1985; Wandel, Peterson and Malkan 1999; fig. 1 above) eq. 21 gives

$$E_{eff} \approx 17\tau_L^{-1/2}(\eta/0.1)^{-1/4}M_8^{-1/4}eV, \quad (22)$$

similar to the result obtained from accretion disk models below.

5.3. Effective Temperature Models for an accretion disk

In the framework of the thin accretion disk model, we consider four models for determining the effective temperature.

a. The inner disk black body temperature

When the disk is nearly black body up to the inner edge, we can approximate the spectrum by black body emission near the maximum-emissivity radius, which gives

$$E_{max} \approx (3 \text{ eV})kT_{BB}(5R_s) = 10(\dot{m}/M_8)^{1/4}. \quad (23)$$

As discussed in sec. 3 above, this model applies to the “ β ” disk and to low accretion rates ($\dot{m} < 0.1$) in the α disk. A similar expression (eq. 13) applies to the Kerr disk.

b. The inner disk radiation-pressure temperature

This model applies to high accretion rates ($\dot{m} > 0.1$) in the α disk, provided the inner disk maintains the temperature profile given by the thin-disk solution. The temperature in the inner, radiation dominated region is given by (Sakura and Sunyaev 1973)

$$T_{rad}(r) \approx (2 \times 10^5 \text{ K})(\alpha M_8)^{-1/4}r^{-3/8}[1 - (6/r)^{1/2}]^{1/4}. \quad (24)$$

Substituting the maximal-emissivity radius $r = 5$ gives

$$E_{max} \approx (4 \text{ eV})(\alpha M_8)^{-1/4} \quad (25)$$

and a higher value for a Kerr black hole. The gas-radiation pressure boundary - taking as T_{max} the temperature at the inner boundary between the black body and the radiation-dominated disk

c. The black body -radiation boundary temperature

In this case the effective temperature is taken at the boundary between the intermediate and inner disk regions, $r_{mi} \approx 10(\alpha M_8)^{0.1}\dot{m}^{0.76}$.

The energy of the peak in the spectrum is then derived by substituting r_{mi} into eq. 24, which gives

$$E_{max} \approx 2(\alpha \dot{m} M_8)^{-0.3} \text{ eV}. \quad (26)$$

This model is adequate in the case of a high accretion rate $-\alpha$ disk when the inner disk does not follow the thin disk model but establishes a stable hot solution (e.g. Wandel and Liang 1991).

d. The “photospheric” temperature

In this model we consider as the disk effective temperature the temperature at the radius where the disk becomes effectively optically thin. The effective optical depth in the disk is given by

$$\tau_* = h\rho(\kappa_{es}\kappa_a)^{1/2},$$

where h and ρ are the disk vertical scale-height and density, respectively, and κ_{es} and κ_a are the electron-scattering and absorption opacities. Equating τ_* to unity and eliminating T and r by using the temperature profile $T(r)$ gives

$$E_{max} \approx 2\alpha^{-0.4}(\dot{m}M_8)^{-0.26} \text{ eV.} \quad (27)$$

Note that the last two models give very similar results.

6. The Line Emissivity

The equivalent width of an emission-line is actually the ratio between the luminosity in the line and the continuum luminosity at the emission-line frequency.

The line luminosity is determined by the photoionizing flux, by the covering factor of the line-emitting gas and by the line emissivity which is a function of the flux of ionizing photons and the density. The differential line luminosity emitted from a thin shell can be written as

$$dL_{line} = L_{ion} \frac{df}{dr} j_{line}(r) dr \quad (28)$$

where df/dr is the differential covering factor, and $j_{line}(Q, n)$, the line relative surface emissivity (or reprocessing efficiency), is a function of the flux of ionizing photons ($Q = L_{ion}/4\pi r^2 c < E >$), the density (n). $< E >$ is the weighted mean energy per ionizing photon. The line luminosity is then found by integrating eq. 28 over radius

$$L_{line} = L_{ion} \int \frac{df}{dr} j_{line} [Q(r), n(r)] dr \quad (29)$$

In order to relate the line luminosity to the ionizing spectrum, we need first to express the line luminosity in terms of the ionizing luminosity and spectrum. The emissivity of several lines has been charted for large portion of the $Q - n$ (flux and density) plane using the CLOUDY photoionization code in a slab geometry (Baldwin *et al.* 1994, Korista *et al.* 1995). These authors find that some lines, in particular CIV $\lambda 1549$ and OVI $\lambda 1094$ have a particularly simple emissivity

structure, with the emissivity peaking strongly (and being approximately constant) along the diagonal $Q/n = \text{const.}$, that is, for the ionization parameter (defined by $U = Q/n$) being constant, $U \approx U_o$.

Approximating

$$j(Q, n) \approx j_o \delta(U - U_o)$$

(the locally maximally emitting model) the line luminosity can then be written as

$$L_{\text{line}} \approx L_{\text{ion}} f_{\text{eff}} j_o, \quad (30)$$

f_{eff} is the effective covering factor, given approximately by integrating df/dr convolved with $j(r)$ over the emitting layer, and the effective radius (e.g. for calculating f_{eff} is given by the condition $U(r_{\text{eff}}) = U_0$, or

$$r_{\text{eff}} \times [n(r_{\text{eff}})]^{1/2} \approx \left(\frac{L_{\text{ion}}}{4\pi U_0 < E > c} \right)^{1/2}. \quad (31)$$

7. Relating the equivalent width to M and L

From the definition of the equivalent width we have $EW_I \approx L_I / L_c$, where I denotes the line in question and L_c is the continuum flux at the frequency corresponding to that line. In section 5 we have seen that the thermal UV spectrum from the accretion disk has a strong dependence on the effective surface temperature of the disk, and that for a variety of models the functional dependence of the effective photon energy on the black hole mass is approximately

$$E_{\text{eff}}(M) \approx (3 - 6 \text{ eV}) M_8^{-1/4} \quad (32)$$

where the range in the coefficient accounts for the uncertainty in the parameters \dot{m} and α (for the accretion disk models) or η and τ_L (for the variability-temperature relation).

7.1. The Temperature-Luminosity Relation

A more direct relation can be obtained with the luminosity (which is what we actually need in the context of the Baldwin effect).

The variability-temperature relation gives $E_{\text{eff}} \approx (10 \text{ eV})(\tau_L/1\text{day})^{-1/2} L_{46}^{-1/4}$, For the accretion disk models we express M and \dot{m} in terms of L . Since, from the definition of \dot{m} we have $\dot{m}M_8 = 1.3 \times 10^{46} L_{\text{bol},46} \text{erg/sec} \approx (10 - 20)L_{\text{opt},46}$, so that

$$(\dot{m}M_8)^{1/4} \approx 2L_{46}^{1/4}$$

The inner black body model (eq. 23) gives

$$E_{eff} \approx (4 \text{ eV})(\dot{m}/0.1)^{1/2}(\alpha/0.1)^{-1/4}L_{46}^{-1/4}$$

the radiation-pressure model (eq. 25) -

$$E_{eff} \approx (8 \text{ eV})(\dot{m}/0.1)^{1/4}(\alpha/0.1)^{-1/4}L_{46}^{-1/4}$$

two last accretion disk models (eqs. 26, 27) can be combined into a single expression

$$E_{eff} \approx (2 \text{ eV})\alpha^{-1/3}\dot{m}^{-1/4}M_8^{-1/4}$$

which gives

$$E_{eff} \approx (3 \text{ eV})(\alpha/0.1)^{-1/3}L_{46}^{-1/4}.$$

Note that the accretion disk models are not including Comptonization by a hot gas, which is likely to increase E_{eff} , so they are probably underestimating E_{eff} .

Combining the variability and accretion disk estimates we can write

$$E_{eff}(L) \approx E_c L_{46}^{-1/4} \quad (33)$$

with $E_c \sim (10 - 20)\text{eV}$, allowing for a range in the parameters α , τ_L and \dot{m} . This theoretical result is consistent with the empirical distribution of E_{co} independently found from the BLR data (fig. 1), and with direct observations of the far UV spectrum of AGN, which show that the SEDs of several AGN observed with IUE and HUT peaks at 1000Å (Zheng *et al.* 1997, Kriss *et al.* 1999).

7.2. Power Law Continuum

The observed SEDs suggest that the decrease in the far UV is a power law ($\sim \nu^{-(1.5-2)}$) rather than exponential. Assuming a UV spectrum of the form

$$L_\nu \sim \nu^{-1} \text{ for } h\nu < E_b$$

$$L_\nu \sim \nu^{-\alpha} \text{ for } h\nu > E_b$$

and $E_I < E_b < E_{ion}$ gives

$$EW_I \propto L_{ion}/\nu L_\nu(E_I) \approx (E_b/E_{ion})^{\alpha-1}$$

because the line luminosity is proportional to the ionizing luminosity $L_{ion} \approx \nu L_\nu(E_{ion})$.

Taking $E_b = E_{eff}$ we then have

$$EW_I \propto L_{ion}/L_I \approx (E_{ion}/E_b)^{-1} \approx (E_c/E_{ion})^{-1}L^{-(\alpha-1)/4}. \quad (34)$$

For $\alpha \sim 1.5 - 2$ (Zheng *et al.* 1997) this gives $EW \propto L^{-\gamma}$ with $\gamma \sim 0.13 - 0.25$.

While for a pure power law, this would imply the same slope for all lines, if the spectrum is curving to steeper slopes at higher photon energies (as could be the case for a partially Comptonized Wien continuum), lines with higher ionization potential (e.g. OVI) would have a steeper slope and vice versa - also consistent with the data.

7.3. Wien Continuum

From eq. 12

$$EW_I = L_{\nu ion}/L_{\nu I} j_0 f_{eff} \propto (E_I/E_{ion})^{1/3} \exp[(E_I - E_{ion})/E_{eff}] \quad (35)$$

Combining these two equations we have

$$EW_I \propto \exp\left(\frac{E_I - E_{ion}}{E_c L_{46}^{-1/4}}\right) \quad (36)$$

Subject to these uncertainties, we can try to estimate the Baldwin effect quantitatively.

For the CIV $\lambda 1546$ line $(E_I - E_{ion}) = (8 - 48)$ eV = -40 eV, which gives

$$\dots/aasn/EW_{CIV} = EW_{CIV} \exp(-40 \text{ eV} E_c^{-1} L_{46}^{1/4}). \quad (37)$$

The coefficient can be determined by normalizing the model to the low luminosity end to the data, where the equivalent width seems to be independent of the luminosity. Although the data has a large dispersion, part of it is probably due to intrinsic variability. Plotting the time average equivalent width vs continuum luminosity gives a significantly smaller dispersion (Kinney, Rivolo and Koratkar 1990, fig 4). From these data we get $EW_{CIV} = 120 \text{ \AA}$.

The slope of the Baldwin effect predicted by eq. 37 is

$$\frac{d\ln(EW_{CIV})}{d\ln L_{46}} = -10 E_c^{-1} L_{46}^{1/4} \quad (38)$$

For $E_c = 20 \text{ eV}$ this gives a slope of $\sim 0.5 L_{46}^{1/4}$.

Fig. 2 shows the data referenced above, along with the model prediction (eq. 37) as a dashed curve. We note that the decrease in the equivalent width predicted by eq. 37 is too large for luminous quasars.

The Baldwin Effect - Data and Models

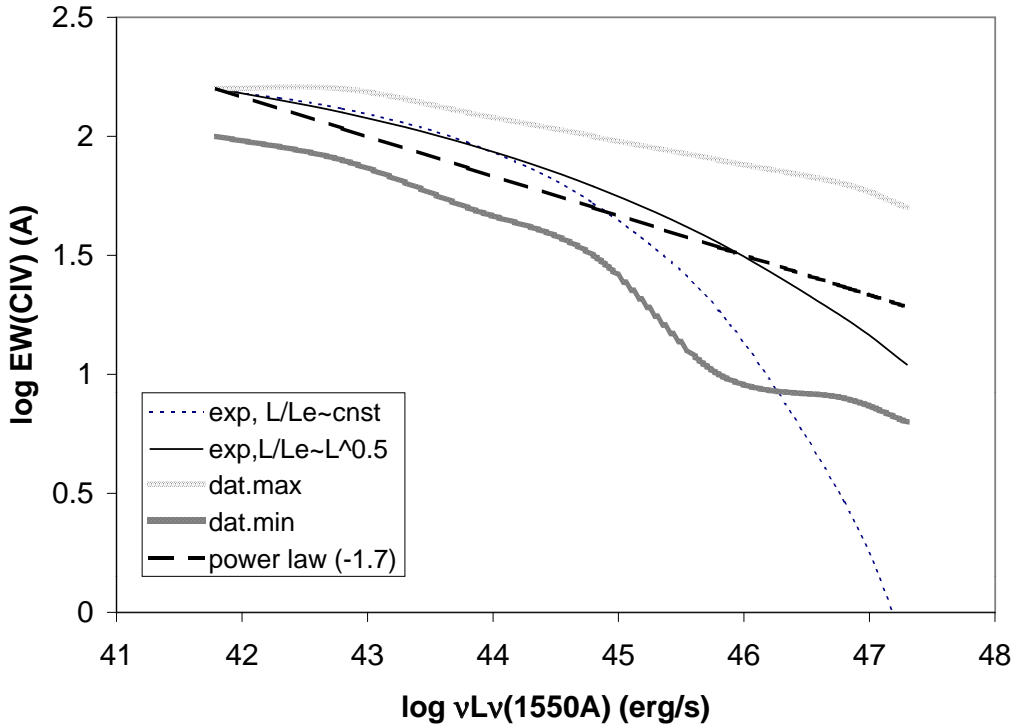


Figure 2. The Baldwin effect (equivalent width of CIV vs. the monochromatic continuum luminosity at 1550Å. The fuzzy thick curves indicate the dispersion of the data, taken from Kinney, Rivolo and Koratkar (1990). The smooth curves indicate the prediction of the models derived in this work: heavy dashed - a power law ionizing spectrum, $L_\nu \sim \nu^{-1.7}$, dotted - with constant L/M (eq. 37 with $E_c = 20$ eV) , solid with $L/M \propto L^{1/2}$ (eq. 39).

This is a result of our assumption that $L/M \sim constant$. Actually, as discussed in section 4 the L/M ratio appears to be correlated with luminosity (see fig. 1), with the exception of NLS1. A similar result is obtained by Wandel and Petrosian (1988) and (although on a small range in luminosity) by Wandel, Peterson and Malkan (1999, fig. 4).

From fig. 1 we adopt an approximate relation

$$L/L_{Edd} \approx 0.1L_{46}^{1/2}.$$

Combining this with eqs. 15 yields

$$E \approx (20 \text{ eV})L_{46}^{-1/8}$$

which gives for the equivalent width

$$EW_{CIV} = EW_{CIV} \exp(-2L_{46}^{1/8}). \quad (39)$$

This result is shown by the solid curve in fig. 2, which is consistent with the observed Baldwin effect .

For Ly α we have $E_I - E_{ion} = 9.2 - 13.6 = 4.4\text{eV}$, which gives

$$\frac{d\ln(EW_{Ly\alpha})}{d\ln L_{46}} = -1.1E_c^{-1}L_{46}^{1/4}. \quad (40)$$

which is consistent with the weaker Baldwin effect found for the Ly α line (Kinney, Rivolo and Koratkar 1990).

8. Discussion

8.1. Comparison with the Data: Luminosity and Energy dependence

Our derivation predicts a weak luminosity dependence of the Baldwin effect . While this dependence (eq. 38) on luminosity, indicating a slow increase of the Baldwin effect (or a decrease of the slope of the line luminosity vs. continuum luminosity) for very luminous quasars is not obvious from the data, it cannot be ruled out either, because of the large scatter. When the scatter is reduced by averaging multiple observations of the same object, (e.g. fig. 4a in Kinney, Rivolo and Koratkar (1990) the resultant Baldwin effect seems to suggest an increase the slope of EW plotted vs. L at high luminosities.

We have seen however, that the increase in the Baldwin effect predicted by eq. 38 is too strong at the highest luminosities. When the increase of the Eddington ratio with luminosity is taken into account, the model can fit the CIV data for the highest energies, for $E_c \approx 20\text{eV}$. This value may be obtained for a disk extending to the last stable orbit or by including Comptonization.

Alternatively, the excess effect could be compensated by the fact that the parameters \dot{m} and τ_L may depend on luminosity; If \dot{m} increases with L (as indicated in Wandel, Peterson and Malkan 1999) or the variability timescale increase with L less than linearly, E_c will increase with luminosity, compensating for the weak luminosity increase. An additional uncertainty is due to the unknown dependence of the emissivity (which we assume to be constant) on L , which may be influenced, among other factors, by the covering factor.

8.2. Comparison with the Data: the Baldwin effect in other lines

The Baldwin effect has been observed also for other lines. Our model predict a strong dependence of the Baldwin effect on the ionization energy. It is interesting to see whether this prediction could reproduce observed strength of the Baldwin effect in different lines. Fig. 4b of Kinney, Rivolo and Koratkar (1990) shows a much weaker effect for Ly α , and in particular for low luminosity objects ($L > 10^{46}$ erg/sec) the Ly α data are consistent with a constant equivalent width , which is predicted by our model (eq. 40).

By the same token, our model predicts that lines with a higher ionization potential like OVI) should have a stronger Baldwin effect , which is also observed (Korista *et al.*1995).

As the emissivity of CIV and OVI has a similar characteristic distribution in the $Q - n$ plane, one could expect a similar Baldwin effect for the two lines, which is indeed observed. The lack of that sharp feature in the emissivity of lines such as Ly α and H β (Korista *et al.*1998a) could explain the fact that these lines do not show a significant Baldwin effect or only a weak one. Such a specific functional form can be predicted by assuming an explicit radial distribution of the density and covering factor. This the expected functional form of the Baldwin effect could provide an observational test of the main suggestion of the paper.

8.3. Normalization

We have reproduced the Baldwin effect from the basic relations between black hole mass, accretion disk temperature combined with the line emissivity. It would be of interest to estimate the normalization for the proportionality relationship found, which would enable a quantitative prediction of the expected Baldwin effect . However, the relation between the emission line luminosity and the ionizing continuum shape depend on the unknown density profile of the line emitting gas, and on the unknown differential covering factor, as discussed in section 5. In the absence of more detailed data on the radial distribution of the line emitting gas, further analyses is limited to qualitative predictions, for which the positive correlation with the radiation temperature demonstrated in sections 5-7 is sufficient. A more explicit dependence predicted by photoionization models can be obtained using the equations derived in sections 5 and 6, if the radial distribution (characterized by $n(r)$ and $df(r)/dr$) are known.

9. Summary

We suggest that the Baldwin effect is a result of the distribution of black hole masses combined with the thermal nature of the line-driving ionizing continuum. Using the variability-black body relation, or alternatively the thin accretion disk spectrum, we derive an analytical estimate for the dependence of the continuum spectrum on the black hole mass and show that the

ratio of ionizing continuum to the continuum luminosity near the lines (related to the equivalent width) is slowly decreasing with increasing mass. We find that for a model-independent black body temperature and for most variants of the thin accretion disk model the equivalent width decreases with increasing continuum luminosity, reproducing the observed Baldwin effect.

Stimulating discussions with Jack Baldwin during the meeting "Quasars as Standard Candles in Cosmology" at La Serena, Chile, triggered this work. I also acknowledge valuable discussions with Gary Ferland, Matt Malkan and Vahé Petrosian, the contribution of an anonymous referee, and the hospitality of the Astronomy Department at UCLA and Stanford University.

REFERENCES

Baldwin, J.A. 1977, ApJ, 214, 679.

Barr, P. & Mushotzky, R.F. 1986, Nature, 320, 421

Boller, Th., Brandt, N. and Fink, V. 1996, A& A 305, 53

Boroson, T. and Green, R.F. 1992, ApJS 80, 109

Czerny, B, Witt,H.J. and Zycki,P.T. 1996, astro-ph/9609180.

Edelson, R. and Nandra, K. 1999, ApJ Haardt, F. , Maraschi, L. and Ghisellini, G. 1994, ApJ, 432, L95

Kinney, A.L.,Rivolo A.R. and Koratkar A.P. 1990, ApJ357, 338.

Korista, K. *et al.*1995 ApJS97, 285.

Korista, K. *et al.*1998 in Structure and Kinematics of Quasar Broad Line Regions, eds. C.M. Gaskell *et al.*ASP

Kriss, G. 1999,

Laor, A. 1990, MNRAS, 246, 369.

Malkan, M.A. 1990, in IAU Colloquium no. 129, "Structure and Emission Properties of Accretion Disks", eds. C. Bertout et.al., Editions Frontiers: Paris, p. 165.

Mathews, W.G. and Ferland, G.J. 1987, ApJ, 323 , 456.

Barr, P. and Mushotzky, R.F. Nature,

Netzer, H. 1990 in "Active Galactic Nuclei", Saas-Fee Advanced Course 20, eds. T.J.-L. Courvoisier and M. Major, Springer Verlag, Berlin, p. 57.

Peterson, B.M."An Introduction to Active Galactic Nuclei" Cambridge Univ. Press, 1997.

Rees, M., Netzer H., Ferland, G.J. 1989. ApJ, 347, 640.

Shields, J. and Osmer, P. 1998 in "Quasars as Standard Candles for Cosmology", La Serena, Chile, ed. G. Ferland, ASP.

Sun, W.H. and Malkan, M.A. 1989, ApJ, 346, 68.

Ulrich, M.H., Maraschi, L. and Urry, M. 1997 ARAA

Wandel, A. 1997, ApJ430, 131.

Wandel, A. 1998, in Structure and Kinematics of Quasar Broad Line Regions, eds. C.M. Gaskell *et al.* ASP, astro-ph/9808171.

Wandel, A. and Boller, Th. 1998, A&A, 331, 884.

Wandel, A. and Liang, 1991, ApJ, 380, 84.

Wandel, A. and Mushotzky, R.F. 1986, ApJ, 306, L61.

Wandel, A., Peterson, B.M. and Malkan, M.A. 1999, ApJ, in press.

Wandel, A. and Petrosian, V. 1988, ApJ, 329, L11.

Wandel, A. and Yahil, A. 1985, ApJ, 295, L1.

Wu, C.C, Bogges, A. and Gull, T.R. 1983 /apj 266, 28.

Zheng, W., Kriss, G.A., Telfer, R.C., Grimes, J.P., and Davidsen, A.F. 1997, ApJ, 475, 469.